

# Fission properties of the BCPM functional

Samuel A. Giuliani\* and Luis M. Robledo†

*Departamento de Física Teórica, Universidad Autónoma de Madrid, E-28049 Madrid, Spain*

Fission dynamics properties of the Barcelona-Catania-Paris-Madrid (BCPM) energy density functional are explored with mean field techniques. Potential energy surfaces as well as collective inertias relevant in the fission process are computed for several nuclei where experimental data exists. Inner and outer barrier heights as well as fission isomer excitation energies are reproduced quite well in all the cases. The spontaneous fission half lives  $t_{sf}$  are also computed using the standard semiclassical approach and the results are compared with the experimental data. The experimental trend with mass number is reasonably well reproduced over a range of 27 orders of magnitude. However, the theoretical predictions suffer from large uncertainties when the quantities that enter the spontaneous fission half life formula are varied. Modifications of a few per cent in the pairing correlation strengths strongly modify the collective inertias with a large impact on the spontaneous fission lifetimes in all the nuclei considered. Encouraged by the quite satisfactory description of the trend of fission properties with mass number we explore the fission properties of the even-even uranium isotope chain from  $^{226}\text{U}$  to  $^{282}\text{U}$ . Very large lifetimes are found beyond  $A=256$  with a peak at neutron number  $N=184$ .

## I. INTRODUCTION

Fission is a physical phenomenon taking place in heavy atomic nuclei that leads to the disintegration of a parent nucleus into two or more emerging fragments. It involves the evolution of the nucleus from its ground state to scission going through a variety of intrinsic shapes that cover a wide range of different intrinsic deformation parameters [1–4]. Fission properties depend upon the competition between the surface energy term coming from the strong nuclear interaction and the Coulomb repulsion and therefore they are often used as constraints and/or guidance to refine the parameters of effective nuclear interactions. A typical example is the D1S parametrization of the Gogny [5] force with parameters fine tuned to reproduce the fission barrier of  $^{240}\text{Pu}$  [6]. More recently fission related constraints have been used with Skyrme interactions to define the UNEDF1 parametrization [7, 8].

The gross features of fission can be understood from a mean-field perspective using the Hartree-Fock-Bogoliubov (HFB) theory [9] and therefore it is not surprising the large amount of studies devoted to this subject with Skyrme interactions [8, 10–12], Gogny ones [6, 13–19] or based on the relativistic mean field [20–22]. Fission observables also depend on the inertia of the system to the relevant collective degrees of freedom and therefore they are sensitive to pairing correlations. As a consequence, fission is a good testing ground to test both the theories and interactions commonly used in nuclear structure. In addition, the theoretical understanding of fission is relevant to other areas outside traditional nuclear physics like safe energy production with nuclear reactors, radioactive waste degradation or the nucleosynthesis of heavy elements in the explosive galactic environments through the  $r$ -process. Last but not least, a

better understanding of fission could open the door to a better estimation of magic numbers and hence extra stability of super-heavy nuclei beyond  $Z=114$ . In this paper we explore the ability of a newly proposed energy density functional (EDF) denoted as Barcelona-Catania-Paris-Madrid (BCPM) [23] to describe fission.

The BCPM is a recent parametrization of the BCP EDF [24–27] devised for nuclear structure calculations. Its free parameters have been adjusted to reproduce the binding energies of even-even nuclei all over the nuclide chart, including deformed ones. Instead of the more traditional approaches where some central potential form is guessed (contact, gaussian, Yukawa, etc) and used afterwards to fit nuclear matter properties and/or the nuclear matter equations of state EoS (both symmetric and neutron), in the BCPM functional we start from a microscopic EoS that is fitted by means of a low order polynomial in the density. That polynomial fit is translated to a finite nuclei EDF just by replacing the nuclear matter density by the density of the finite nucleus. This procedure is inspired by the local density approximation (LDA) and is common practice in practical applications of the Kohn-Sham theory in condensed matter physics. The EDF is supplemented with a finite range surface term, a contact spin-orbit interaction of the same form as in Skyrme or Gogny forces, the Coulomb interaction and finally, a density dependent zero range pairing interaction [28] with strengths fitted to reproduce Gogny’s neutron matter pairing gap. The parameters of the functional (essentially those of the finite range surface term plus some freedom in the polynomial fit to fine tune the binding energy per nucleon) are fitted to reproduce binding energies of the 518 even-even nuclei of the 2003 mass table evaluation of Audi and Wapstra. The properties of the interaction concerning quadrupole, octupole and fission dynamics have also been explored [23]. As shown below, the BCPM functional gives reasonable results for fission observables including spontaneous fission half lives, fission isomer excitation energies, inner and outer barrier

\* sam.and.giuliani@gmail.com

† luis.robledo@uam.es

heights and mass distribution of fragments. We have also shown that those results could be improved by slightly modifying the amount of pairing correlations, either by modifying the pairing strengths or by going beyond the mean field approximation to restore the particle number symmetry broken by the HFB procedure. As a consequence of the satisfactory performance of BCPM in describing fission, we have explored fission properties of the uranium isotopic chain from proton drip line to the neutron drip line.

## II. METHODS

Both the BCPM energy density functional [23] and its predecessor BCP [24] are made of a bulk part which is determined by fully microscopic and realistic calculations of symmetric and neutron matter equations of state [29, 30] as in the LDA of condensed matter physics. The two equations of state (symmetric and neutron matter) given as a function of the nuclear density are parametrized by low order polynomials of the densities. To account for finite size effects related to the surface energy, a phenomenological finite range gaussian interaction is included. In addition, the Coulomb interaction and the spin-orbit term are taken exactly as in the Skyrme or Gogny forces. To deal with open-shell nuclei we include in the BCPM and BCP functionals a zero range density-dependent pairing interaction fitted to reproduce the nuclear matter gaps obtained with the Gogny force [28]. The calculations in finite nuclei are carried out with a modification of the HFBaxial computer code developed by one of the authors [31].

To describe fission we follow the usual procedure based on the mean field approach with pairing correlations: the Hartree-Fock-Bogoliubov (HFB) theory with constraining fields. As constraining operators we have used mainly the axially symmetric quadrupole moment operator  $Q_{20} = z^2 - \frac{1}{2}(x^2 + y^2)$  although some exploratory calculations have also been performed with the octupole  $Q_{30}$  and hexadecapole  $Q_{40}$  moment operators and the necking operator  $Q_N(z_0) = \exp(-(z - z_0)^2/C_0^2)$ . Axial symmetry is preserved in the calculations because of the high computational cost involved in the release of this restriction. We are aware of the relevance of triaxiality specially in the height of the inner fission barrier but its effect is merely quantitative and to a much lesser extent, qualitative. On the other hand, reflection symmetry is allowed to break at any stage of the calculation permitting octupole deformation and asymmetric fission. As a consequence of the breaking of the parity symmetry we are forced to constraint the center of mass to the origin as to prevent spurious solutions corresponding to a translation of the nucleus as a whole. The quasiparticle creation and annihilation operators of the HFB theory are expanded in a harmonic oscillator basis (HO) preserving axial symmetry and containing HO states with  $J_z$  quantum numbers up to  $35/2$  and up to 26 quanta

in the  $z$  direction. The basis contains over 3000 levels but time reversal invariance and the axial block structure reduces the computational complexity to a manageable level. The two lengths characterizing the HO basis,  $b_\perp$  and  $b_z$ , have been optimized in a few nuclei for each value of the quadrupole moment. For the others the oscillator lengths computed for nearby nuclei are used. As the number of HFB configurations for each nucleus is large, a robust and fast gradient-like algorithm to solve the HFB equations is used [9, 32]. The most evident advantage of this method is the way it handles the constraints, which allows an easy generalization to an arbitrary number of them.

The spontaneous fission lifetime formulas Eqs 4 and 5 below, depend crucially on the theory of the collective mass  $B(Q_{20})$ . We shall use two methods to calculate it and compare in our results. The first is the well-known cranking approximation to the Adiabatic Time dependent HFB approximation [9]. The resulting mass is expressed in terms of the moments  $M_{(-n)}$  of the generating field  $Q_{20}$

$$M_{(-n)} = \sum_{\alpha>\beta} \langle 0|Q_{20}|\alpha\beta\rangle \frac{1}{(E_\alpha + E_\beta)^n} \langle \alpha\beta|Q_{20}|0\rangle \quad (1)$$

as

$$B(Q_{20}) = \frac{1}{2} \frac{M_{-3}}{(M_{-1})^2}. \quad (2)$$

Here  $|\alpha\beta\rangle$  are distinct 2-quasiparticles excitations and  $E_\alpha + E_\beta$  is the excitation energy, neglecting the quasiparticle-quasiparticle interaction (cranking approximation [33–35]).

An alternative method to calculate the mass is based on the gaussian overlap approximation to the generator coordinate method (GCM). It is often simplified to obtain the expression

$$B(Q_{20}) = \frac{1}{2} \frac{M_{-2}^2}{(M_{-1})^3}. \quad (3)$$

We shall calculate the lifetimes with both Eq 2 and 3 and compare. We note that Ref [36] compares several forms of the mass, including Eq 2 and 3, in the context of the Skyrme functionals. It is also important to mention the dependence of the mass with the amount of pairing correlations: it has been shown in Refs [4, 37] that the mass is inversely proportional to some power of the pairing gap. It means that the stronger the pairing correlations are the smaller the mass is.

Zero point energy corrections to the HFB energy  $\epsilon_0(Q_{20})$  are also considered in the ATDHFB and GCM approaches. In addition, the rotational energy correction computed following the phenomenological prescription of Ref [38] is also subtracted. This correction is very important to the shape of the potential energy as its value increases with deformation and can reach several MeV for large deformations.

The spontaneous fission half life is computed with the standard WKB formalism of quantum mechanics. In the WKB formalism the  $t_{sf}$  is given (in seconds) by the formula

$$t_{sf} = 2.86 \cdot 10^{-21} (1 + \exp(2S)) \quad (4)$$

The action  $S$  along the  $Q_{20}$  constrained path is given by

$$S = \int_a^b dQ_{20} \sqrt{2B(Q_{20})(V(Q_{20}) - (E_{GS} + E_0))}. \quad (5)$$

where the integration limits correspond to the classical turning points for the energy  $E_{GS} + E_0$ . For the collective quadrupole inertia  $B(Q_{20})$  we have used both the ATDHF and the GCM expressions. The results obtained with the two different theories can differ in several orders of magnitude as the ATDHF mass is known to be a factor in between 1.5 and 2 larger than the GCM mass. The potential energy  $V(Q_{20})$  is given by the HFB mean field energy corrected by zero point energies as described above,  $V(Q_{20}) = E_{HFB}(Q_{20}) - \epsilon_0(Q_{20}) - E_{Rot}(Q_{20})$ . Finally, an additional parameter  $E_0$  is added to the ground state energy  $E_{GS}$ . It is meant to represent the true ground state energy obtained after considering quantal fluctuations in the quadrupole degree of freedom. This quantity could be estimated to be half of the square root of the curvature around the minimum divided by the collective inertia but it is often taken as a free parameter or kept fixed at some reasonable value. We have followed the later approach with  $E_0 = 1.0$  MeV and estimated the impact of considering a larger value by repeating the calculations with  $E_0 = 1.5$  MeV.

The spontaneous fission half life obtained in this way is subject to several uncertainties that can lead to differences of several orders of magnitude. The uncertainties are: 1) the height of the inner fission barrier gets reduced when triaxial shapes are allowed in the mean field calculation. The amount of reduction is typically of a couple of MeV, but it can show some isotopic variation (see [15] for a recent account in the actinide region); 2) the value of  $E_0$ . It can also make a difference in  $t_{sf}$  specially for long lived isotopes where the fission barrier is wide. The reason is that the value of  $E_0$  alters the classical turning points; 3) the values of the correlation energy corrections to the HFB energy included in  $V(Q_{20})$ . The values are computed under certain assumptions and approximations and a better estimation of their values can lead to some changes to  $V(Q_{20})$ ; 4) the approximations involved in the evaluation of the collective masses can lead to differences of the order of 40 or 50 %; 5) the pairing correlation. It is an important ingredient both in the evaluation of the zero point energy as well as in the evaluation of the collective inertia. As shown below, changes of a few percent in the pairing strength values can lead to changes in the theoretical estimation of the half lives in the range of five to twelve orders of magnitude.

On the other hand, the experimental values of the parameters defining the potential energy of the fission process, namely the inner and outer barrier heights and the

excitation energy of the fission isomer are more robust quantities to compare with as they are not as sensitive to pairing correlations as the other parameters. However, these experimental quantities are obtained by model dependent assumptions that can mask the physical meaning of the parameters. Therefore, although we have compared our values with the experimental ones, we prefer to compare the trends in spontaneous fission life times as a function of  $N$  and  $Z$  rather than the absolute values of the lifetimes themselves. We will also study the impact of changing various quantities entering the WKB formula.

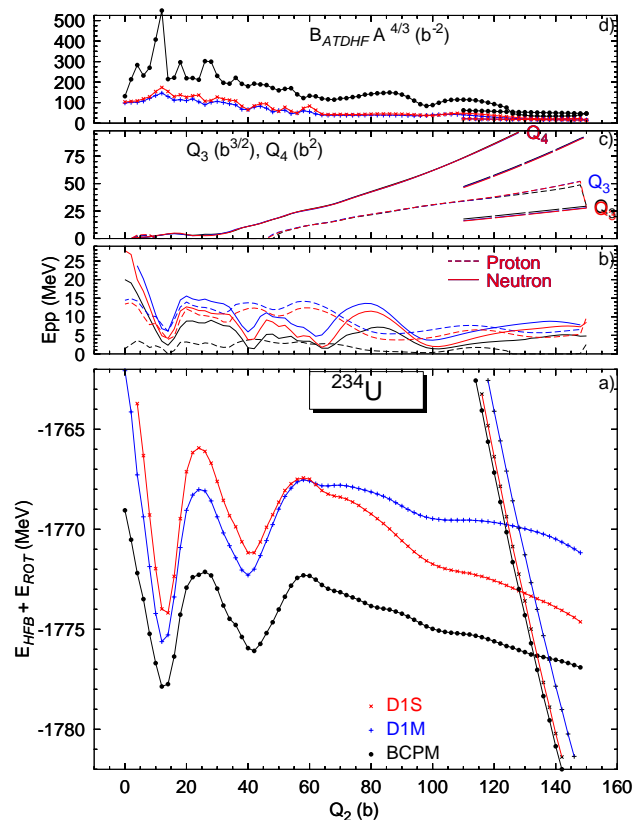


Figure 1. (Color online) Comparison of HFB mean field quantities as a function of the mass quadrupole moment  $Q_{20}$  obtained with three different interactions for the  $^{234}\text{U}$  nucleus. The BCPM EDF (black curves, bullet symbol) as well as the D1S (red, times symbol) and D1M (blue curves, plus symbol) parametrizations of the Gogny force are included. In panel a) the HFB energy is given. In panel b) the particle-particle correlation energy  $E_{pp} = -\text{Tr}(\Delta\kappa)$  is plotted for protons (dashed lines) and neutrons (full lines) for the three different kinds of calculations. In panel c) the octupole and hexadecapole moments are given. Finally, panel d) the ATDHF collective inertia is depicted.

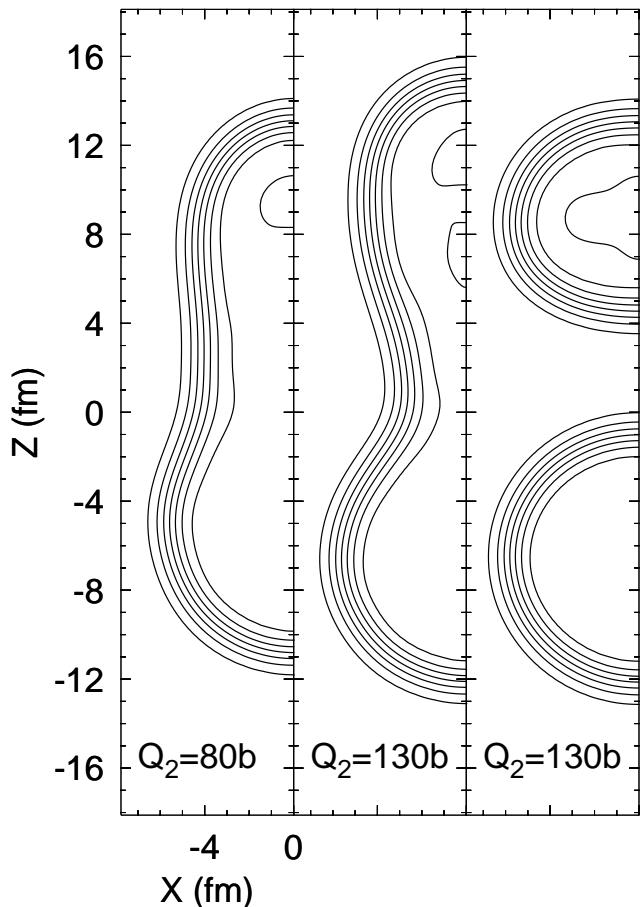


Figure 2. Contour plots of the densities of  $^{234}\text{U}$  for three different quadrupole deformation parameters indicated in each panel. Contour levels correspond to densities between  $0.02 \text{ fm}^{-3}$  and  $0.16 \text{ fm}^{-3}$  in steps of  $0.02 \text{ fm}^{-3}$ . The calculations correspond to the BCPM EDF.

### III. RESULTS

#### A. Comparison with other interactions

Before comparing with the experimental data a comparison with the HFB results obtained with the two Gogny interactions, namely, D1S and D1M, is in order. The Gogny D1S interaction has been used in a thorough study of heavy nuclei properties, including fission, in Ref [15] and it has proved to reproduce quite nicely most of the properties analyzed. On the other hand, the fission properties of D1M [39] have not been analyzed in detail yet but its nice behavior regarding other aspects of nuclear structure like binding energies[39], radii [40] quadrupole [41, 42] and octupole [43] properties make it a good candidate to compare with. As we have already made comparison with D1S concerning fission properties [23] of actinides ( $^{240}\text{Pu}$ ) and super-heavies ( $^{262}\text{Sg}$ ), we will just explore another actinide: the nucleus  $^{234}\text{U}$ .

In panel a) of Fig 1 we compare the HFB energy as

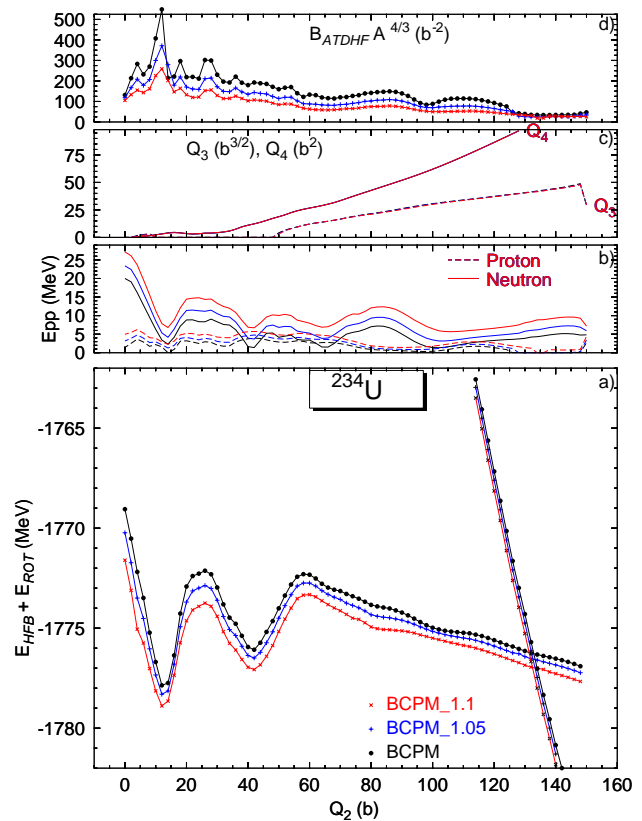


Figure 3. (Color online) Same as figure 1 but for different pairing strengths. The pairing strengths are given in terms of the reference value and a scaling parameter  $\eta$  taking the values 1.00 (the standard calculation), 1.05 and 1.10.

a function of  $Q_{20}$  for the three functionals in the nucleus  $^{234}\text{U}$ . We observe how the shape of the three curves starting at  $Q_{20} = 0\text{b}$  look rather similar up  $Q_{20} = 60\text{b}$ , apart from a constant shift of a few MeV. From there on, the D1M interaction declines more gently than D1S. The BCPM results are in between D1M and D1S but closer to D1M than to D1S. The decline of energy with increasing quadrupole moment is correlated with the surface energy coefficient in nuclear matter which is larger in D1M and BCPM than in D1S [23]. The other three curves only present at large  $Q_{20}$  values correspond to HFB solutions with two well separated fragments. They intersect the one fragment curves at  $Q_{20}$  values around 130 b and they show a fast quasi-linear decrease in energy as the quadrupole moment increases. The charge and mass of each fragment are the ones that lead to the minimum energy for each quadrupole moment. For very large  $Q_{20}$  values the distance between the fragments is larger than the range of the nuclear strong interaction and therefore only the Coulomb repulsion energy between the fragments plays a role. In this two-fragment regime the quadrupole moment is directly linked to the separation distance between fragments [44] and therefore increasing the quadrupole moment is equivalent to separating further away the fragments reducing the total

energy of the system as a consequence of the reduction of Coulomb repulsion. Although the two-fragment curves seems to intersect the one-fragment ones this is just a consequence of projecting out paths in a multidimensional space of collective variables (quadrupole, octupole, hexadecapole, necking, etc) into an one dimensional plot (see below). There is a minimum action path with a ridge connecting both the one and the two fragments curves that goes along the multidimensional space. This path contributes to the action that enters the WKB formula to compute the  $t_{sf}$  half lives. As the determination of this path is cumbersome and its contribution to the action is small we will neglect its contribution to the action. This simplification amounts to consider both curves as really intersecting ones.

A measure of pairing correlations, the pairing interaction energy  $E_{pp} = -\text{Tr}(\Delta\kappa)$ , is shown as a function of the mass quadrupole moment for protons (dashed lines) neutrons (full lines) in panel b) of Fig 1. Again the shape of the curves look rather similar for the three functionals but BCPM yields lower values of  $E_{pp}$  than D1S and D1M. Those lower values correspond to less intense pairing correlations in the BCPM case with a severe quenching of the proton's pairing correlations. In panel c), the octupole and hexadecapole moments as a function of  $Q_{20}$  are given. The results for the three EDFs are very similar, to the extent that they appear as a single curve for many  $Q_{20}$  values. The full curves correspond to the one-fragment solutions whereas the long dashed ones correspond to the scissioned configurations. As mentioned before, the values of the multipole moments of the two kind of curves are quite different and therefore the paths are quite separated in the multidimensional space of parameters. Finally, in panel d) the collective inertia in the ATDHFB approximation is plotted. As in the case of the HFB and particle-particle energies the shape of the curves for the different interactions are quite similar but the BCPM inertia is up to a factor of three larger than the inertias obtained with the Gogny forces. The large value of the BCPM inertia is a direct consequence of the quenched pairing correlations: less pairing correlations imply a lower gap and therefore smaller two quasiparticle energies. As the two quasiparticle energies enter the collective inertia in the denominator, quenched pairing correlations imply enlarged collective inertias. On the other hand, the D1M inertia is around 15 % smaller than the D1S one, consistent again with the quenched pairing correlations in D1M as compared to the D1S ones. The GCM inertias, not depicted, look rather similar in shape to the ATDHFB ones but are a factor of 0.5-0.6 smaller. The inertia for the two fragment solutions corresponds to the reduced mass of the two fragments [44] and is constant with quadrupole deformation.

In the calculation of the  $t_{sf}$  half life with the WKB formula the configuration with the lowest energy is always chosen. This is an approximation that neglects the path in the multidimensional space that connects the one fragment with the two fragment solution and therefore the

$t_{sf}$  obtained are to be considered as lower bounds. On the other hand, triaxiality leads to a reduction of the inner barrier height that is somehow compensated by an increase in the corresponding inertia [15]. This effect has not been included in the present calculation. The values of the  $t_{sf}$  half life obtained for the three EDFs computed with the GCM inertias are  $t_{sf} = 2.3 \times 10^{38}\text{s}$ ,  $4.7 \times 10^{29}\text{s}$  and  $1.3 \times 10^{23}\text{s}$  for BCPM, D1M and D1S, respectively. The large differences observed of up to 15 orders of magnitude can be attributed partly to the difference in the HFB energy curve but mostly to the very different values of the collective inertias. The previous  $t_{sf}$  values have been obtained without taking into consideration the reduction of the inner barrier height as a consequence of triaxiality. Also, increasing the value of the  $E_0$  parameter to 1.5 MeV reduces the half lives by 6, 2 and 4 orders of magnitude respectively. In any case, the values obtained are several orders of magnitude larger than the experimental value of  $4.7 \times 10^{23}$  s expect for Gogny D1S that is very close to experiment. If the ATDHFB inertias are used instead of the GCM ones a much longer lifetimes are obtained:  $t_{sf} = 7.8 \times 10^{52}\text{s}$ ,  $5. \times 10^{40}\text{s}$  and  $2.9 \times 10^{32}\text{s}$  for BCPM, D1M and D1S, respectively. This tendency to produce longer lifetimes when the ATDHFB inertias are used is common to all the isotopes considered in this study. The ATDHFB inertias are typically a factor 1.5 larger than the GCM ones (see Refs [36, 38] for examples) implying a 20 % increase in the action and therefore a 20% increase in the exponent of the lifetimes. This is a source of theoretical uncertainty in the evaluation of  $t_{sf}$  that deserves further investigation. Another source of uncertainty comes from the fact that the inertias are computed in the "cranking approximation" where the energy of elementary excitations is replaced by the sum of HFB quasiparticle energies. The approximation [38] can lead to overestimations in the inertias as large as 40 - 50% for ground state configurations. Given the impact of these effects on the fission observables a better quantitative understanding is highly desirable. In the following, to simplify the presentation, we will consider only the GCM inertias in the evaluation of the lifetimes.

Finally in Fig 2 contour plots of the densities for three values of the quadrupole moment are depicted. They are obtained in calculations with BCPM and differ little from the same quantities computed with D1M and D1S. For the quadrupole moment  $Q_{20}=130$  b two densities, corresponding to the one fragment and two fragment solutions are presented. The two fragment solution shows a spherical fragment that corresponds to  $Z=51.60$  and  $N=82.00$  and an oblate deformed fragment with  $Z=40.40$  and  $N=60.00$ . The non integer proton and neutron number is due to the existence of low density nuclear matter between the two fragments. The oblate and slightly octupole deformed fragment ( $\beta_2 = -0.21$  and  $\beta_3 = 0.03$ ) acquires this shape to minimize the rather large Coulomb repulsion energy (assuming point like fragments the classical repulsion energy amounts to 196 MeV). This is an interesting result because it is commonly assumed [45, 46]

Nucleus	$B_I^{\text{Th}}$	$E_{II}^{\text{Th}}$	$B_{II}^{\text{Th}}$	$B_I^{\text{Exp}}$	$E_{II}^{\text{Exp}}$	$B_{II}^{\text{Exp}}$
$^{234}\text{U}$	5.87	1.78	5.59	4.80	-	5.50
$^{236}\text{U}$	6.49	1.90	6.04	5.0	2.75	5.67
$^{238}\text{U}$	6.99	2.03	6.54	6.30	2.55	5.50
$^{238}\text{Pu}$	6.91	1.85	5.20	5.60	2.4	5.10
$^{240}\text{Pu}$	7.43	2.08	5.69	6.05	2.8	5.15
$^{242}\text{Pu}$	7.72	2.27	6.30	5.85	2.2	5.05
$^{244}\text{Pu}$	7.89	2.47	6.30	5.70	-	4.85
$^{240}\text{Cm}$	6.8	1.2	3.90	-	2	-
$^{242}\text{Cm}$	7.4	1.7	4.5	6.65	1.9	5.0
$^{244}\text{Cm}$	8.0	1.9	5.0	6.18	2.2	5.10
$^{246}\text{Cm}$	8.4	2.3	5.5	6.0	-	4.80
$^{248}\text{Cm}$	8.34	2.04	5.47	5.80	-	4.80
$^{250}\text{Cf}$	8.65	1.25	4.24	-	-	3.8
$^{252}\text{Cf}$	8.35	0.83	3.84	-	-	3.5

Table I. Fission barrier height parameters  $B_I$  (inner) and  $B_{II}$  (outer) as well as excitation energy of the fission isomer  $E_{II}$ . The three parameters are given in MeV. The theoretical values have been obtained from the rotational energy corrected HFB potential energy surface. The experimental values are taken from [49] for the  $E_{II}$  and from [50] for the  $B$ 's.

that the fission fragments can only have prolate shapes.

### B. Varying pairing strengths

In the BCPM functional the pairing interaction is taken as a density dependent contact pairing interaction with strength parameters fixed to reproduce the neutron matter pairing gap of the Gogny force [28]. We have shown in the previous subsection that the particle-particle correlation energy, a quantity related to the amount of pairing correlations, was much smaller for BCPM than for the Gogny forces leading to much larger collective inertias. It is therefore reasonable to investigate the behavior of fission properties as a function of the pairing strength for the same functional. To this end, a parameter  $\eta$  has been introduced as a multiplicative factor in front of the pairing gap field  $\Delta_{kl}$ . For the sake of simplicity we have considered an unique parameter for both protons and neutrons although different parameters will give more flexibility to adjust the experimental data. The outcome of the calculations with  $\eta$  values of 1.05 and 1.10 for the nucleus  $^{234}\text{U}$  are presented in Fig 3. We observe in panel a) that increasing the pairing strength by 10 % ( $\eta = 1.10$ ) leads to an overall gain of the order of 1 MeV in binding energy. For the ground state the 1 MeV energy gains has to be compared to the 1 MeV of pairing correlation energy for the standard BCPM. The gain is even larger (1.6 MeV) for the configuration with  $Q_{20} = 26$  b and corresponding to the top of the inner barrier. However, the standard BCPM pairing correlation energy is 2.06 MeV for that configuration. The net

effect of increasing the pairing strength by 10% is to decrease the inner barrier height ( $B_I$ ) by 0.6 MeV whereas the other parameters, namely the outer barrier height  $B_{II}$  and the fission isomer excitation energy remain more or less the same. The particle-particle correlation energies  $E_{pp}$  shown in panel b) for protons and neutrons increase with increasing  $\eta$  but the slope is larger for neutrons than for protons. The multipole moment values depicted in panel c) do not change at all when the pairing strength is increased and the different values lie on top of each other for different  $\eta$  values. Finally, the impact on the collective inertia is clearly visible in panel d) and is associated to the inverse dependence of the mass on the square of pairing gap [4, 37]. Increasing the pairing strength by 5 % reduces the collective inertia by roughly 30 % whereas a 10 % increase leads to a reduction of 50 %. The consequences of these reductions on the  $t_{\text{sf}}$  are dramatic, decreasing its value by 11 orders of magnitude in going from  $\eta = 1.0$  to  $\eta = 1.05$  ( $t_{\text{sf}} = 8.0 \times 10^{27}$  s) and six additional orders of magnitude in going from  $\eta = 1.05$  to  $\eta = 1.10$  ( $t_{\text{sf}} = 6.7 \times 10^{21}$  s). This result is a clear indication of the very important role played by pairing correlations in the description of fission. The result suggests that experimental fission data could be used to fine tune the pairing strength instead of more traditional approaches based on odd-even staggering. From a theoretical perspective the result also points to the very important role that the correlations associated to particle number symmetry restoration should have in fission dynamics. Restoring particle number symmetry usually leads to larger pairing correlations than the ones present at the mean field level and therefore will have a tremendous impact on fission lifetimes. In this respect it is worth mentioning that the dependence on density of BCPM is on integer powers of the density allowing the use of the regularization techniques suggested to solve some technical problems associated to the evaluation of the energy kernel overlaps required by symmetry restoration theories (see Refs [47, 48] and references therein).

Given the large variability of the lifetimes with the different parameters entering the WKB formula, a direct comparison with the experimental data is meaningless and only comparisons with the trends along a series of nuclei or isotopes, all of them computed in the same conditions, can lead to meaningful conclusions regarding fission properties.

### C. Nuclei with known experimental data

In order to validate BCPM as a functional able to describe fission properties, we have performed calculations for those even-even nuclei where the spontaneous fission half life has been measured. We will also compare the parameters defining the theoretical potential energy surface, namely the inner and outer barrier heights ( $B_I$  and  $B_{II}$ ) and the excitation energy of the fission isomer  $E_{II}$  with available experimental data [49, 50]. It has to be

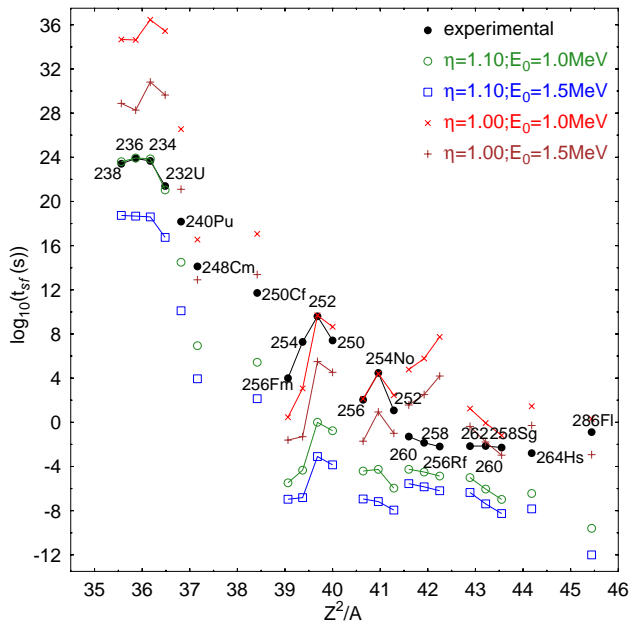


Figure 4. (Color online) Experimental  $t_{sf}$  half lives (bullets) are compared to different theoretical results (open symbols) for several isotopic chains where experimental data exists. The  $t_{sf}$  are plotted as a function of the fissibility parameter  $Z^2/A$ . See text for details.

mentioned that the experimental data for  $B_I$  and  $B_{II}$  [50] is model dependent and therefore less reliable than the pure  $t_{sf}$  data. In table I the experimental and theoretical values for  $B_I$ ,  $B_{II}$  and  $E_{II}$  are given for all nuclei where experimental data exists [49, 50]. The theoretical values have been obtained by considering the HFB energy as a function of  $Q_{20}$  with the rotational energy correction (computed in the way described in the previous section) subtracted. The effect of the zero point energy correction  $\epsilon_0(Q_{20})$  has not been included mainly because it is almost constant as a function of  $Q_{20}$ . We notice that the theoretical predictions for  $B_I$  are typically one or two MeV larger than experiment. This is not surprising as it is well known that the theoretical inner fission barrier is affected by triaxiality and its height typically decreases by one or two MeV when the effect is included in the calculation [15]. Triaxiality is not included at present because we still do not have access to a triaxial code incorporating the BCPM functional but work in this direction is in progress. The situation is slightly better in the comparison with the  $E_{II}$  and  $B_{II}$  values. For them, no significant triaxial effects are expected and the agreement with experiment is better than for the  $B_I$ . In Ref [8] a thorough comparison of these data with various model predictions has been made. In this paper, the RMS deviations for the fission isomer energy and second barrier height are given for several mean field models. The BCPM values  $\sigma(E_{II}) = 0.57$  MeV and  $\sigma(B_{II}) = 0.72$  MeV are similar in magnitude to the ones of UNEDF1 [7] a Skyrme variant specifically tailored to describe fission. This is a

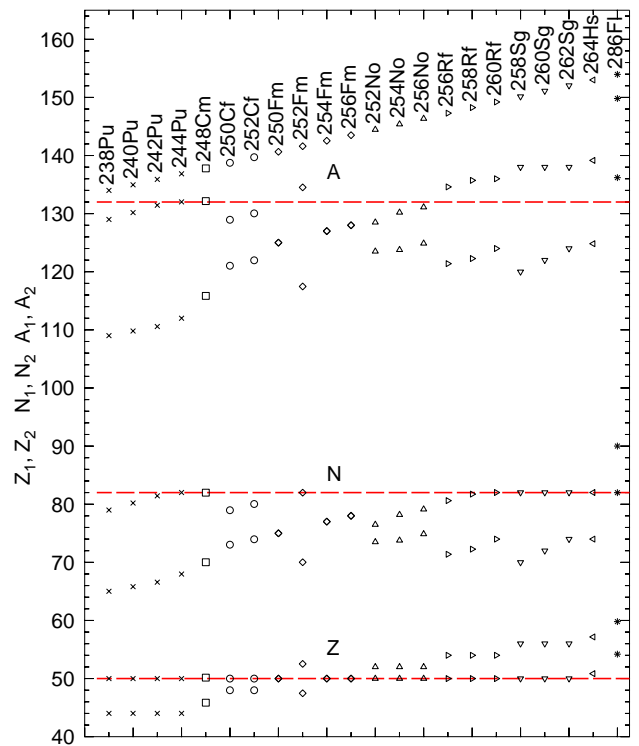


Figure 5. Proton ( $Z_{1,2}$ ), neutron ( $N_{1,2}$ ) and mass number ( $A_{1,2}$ ) of the two fragments emitted by the fission of the parent actinides (perpendicular labels on top). The magic numbers 50 and 82 as well as its sum are highlighted with horizontal lines.

quite satisfactory result taking into account that BCPM does not use any fission data in its fit.

In Fig 4 the theoretical  $t_{sf}$  results obtained for different choices of the  $E_0$  and  $\eta$  parameters are compared to the known experimental values. The experimental  $t_{sf}$  values [51] span a range of 27 orders of magnitude for a mass range  $A=232-286$ . The theoretical predictions, not including triaxial effects and computed with the GCM masses and zero point energies, span an even larger range of values and show a large variability depending upon the choices for the parameters. Focusing on the “standard” theoretical values  $\eta = 1.0$  and  $E_0 = 1.0$  we observe differences with the experiment of up to 16 orders of magnitude for the lighter nuclei that steadily decrease to differences of just a couple of orders of magnitude for the heavier ones. The largest differences are observed for nuclei with higher and wider barriers where the impact of parameters like  $E_0$  is larger. The comparison in isotopic chains indicate that the trend with neutron number compares much better with the experiment than the absolute values. The same conclusion can be extracted from the overall trend with mass number obtained from the table. Therefore, we conclude that the HFB predictions, although subject to large uncertainties due to uncontrolled approximations in the evaluation of the different parameters, can be used to guess with a reasonable



precision the trends of  $t_{\text{sf}}$  with mass number. The second conclusion drawn from this plot is the extreme sensitivity of the half lives to changes in  $\eta$  and  $E_0$ : Increasing the pairing strength by 10% ( $\eta = 1.10$ ) decreases  $t_{\text{sf}}$  by several orders of magnitude. In the Uranium isotopes the reduction is of 12 orders of magnitude bringing the theoretical predictions on top of the experimental data. On the contrary, in the Fm and No isotopic chains the reduction represents only 6 orders of magnitude but worsens the agreement with experiment. On the other hand, the increase of  $E_0$  from 1 MeV to 1.5 MeV also reduces  $t_{\text{sf}}$  by several orders of magnitude, but the reduction is not as severe as with the increase of pairing strength. In the Uranium case, the reduction represents on the average 6 orders of magnitude. Incidentally, the  $t_{\text{sf}}$  values obtained with  $\eta = 1$  and  $E_0 = 1.5$  MeV are in most of the cases very close to the results (not shown) corresponding to  $\eta = 1.05$  and  $E_0 = 1$  MeV.

The sensitivity of the results to the pairing strength demands a theory beyond HFB to describe pairing correlations. A first candidate would be particle number restoration supplemented with configuration mixing using the pairing gaps as collective coordinates. Also the sensitivity to the  $E_0$  parameter justifies an effort to better understand its rationale. This is obviously a task for the future.

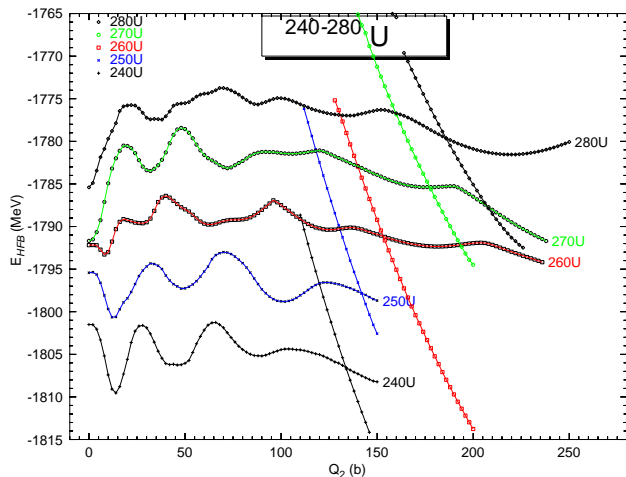


Figure 6. (Color online) HFB energies as a function of the quadrupole moment  $Q_{20}$  for some neutron rich uranium isotopes. The energies have been shifted upwards for the heavier isotopes in order to fit all the curves in a single plot. Along with the one fragment curves starting at  $Q_{20} = 0$  the curves corresponding to the energy of the two fragments resulting of fission are given.

Another important piece of relevant information is the mass distribution of the fission fragments. The mass of the fragments is determined by the nuclear shape in the neighborhood of the scission point. As the scission point is difficult to characterize in a mean field theory that explores just a few degrees of freedom, we have preferred to take a different approach that involves the evaluation of

quasi-fusion configurations. They are obtained by constraining the number of particles in the neck of the parent nucleus

$$Q_N = \langle \phi | \hat{Q}_N(z_0, C_0) | \phi \rangle$$

to a small value and then releasing the constraint to do a self-consistent calculation. Most of the time the self-consistent solution ends up in a solution with two well separated fragments. To make sure that the configuration is the lowest in energy the procedure is repeated with different choices of the neck operator parameters  $z_0$  (position of the neck along the  $z$  direction) and  $C_0$  (the width of the neck distribution). Those configurations are constrained to larger quadrupole moments in order to separate the fragments (please remember that for two fragments the quadrupole moment is proportional to the separation of the fragments [44]). An example of those quasi-fusion curves has already been presented in Fig 1. In Fig 5 the proton (Z) and neutron (N) numbers of the fragments obtained for the actinides considered are given. The Z values of the fragments are mostly determined by the Z=50 magic number except in  $^{252}\text{Fm}$ . Also for the heaviest nucleus considered  $^{266}\text{Fl}$  larger Z values are observed. For neutrons, the magic N=82 seems also to be dominant neutron number but here the exceptions are more numerous. For the plutonium and heavier isotopes the heaviest fragment has a mass number between 130 and 132, ten unit less than the average experimental value of Refs [52, 54]. The discrepancy can be attributed to the lack of quantum fluctuations in our model that can modify substantially the raw mean field numbers [53].

Obviously, the numbers given here are meant to represent the peaks of the fragments' mass distribution which is a broad distribution as a consequence of exchange of particles during the scission process as well as a consequence of neutron evaporation. A better dynamical theory is required (see [53] as an example of such theory) in order to reproduce the experimental broad distribution.

#### D. Neutron rich uranium isotopes

In the previous section we concluded that the description of fission based on the HFB theory is subject to large uncertainties coming from the poor understanding of the way the different quantities entering the WKB formula should be computed. However, we also concluded that the HFB theory is reproducing reasonably well the experimental  $t_{\text{sf}}$  trends with mass number. Encouraged by the result, we have performed calculations in the uranium isotopic chain from the light uranium  $^{226}\text{U}$  up to the neutron drip line corresponding to  $^{282}\text{U}$  with the aim of understanding and analyzing the trends in spontaneous fission half lives and the mass of the emerging fission fragments. To illustrate the results the HFB potential energies for the  $^{240}\text{U}$ ,  $^{250}\text{U}$ ,  $^{260}\text{U}$ ,  $^{270}\text{U}$  and  $^{280}\text{U}$  isotopes are depicted as a function of  $Q_{20}$  in Fig 6. The energies of the heavier isotopes have been shifted by different



amounts of energy (55, 100, 135 and 160 MeV, respectively) to fit all the curves in a single plot. Also the curves corresponding to the two fragment solution with the lowest energy are depicted.

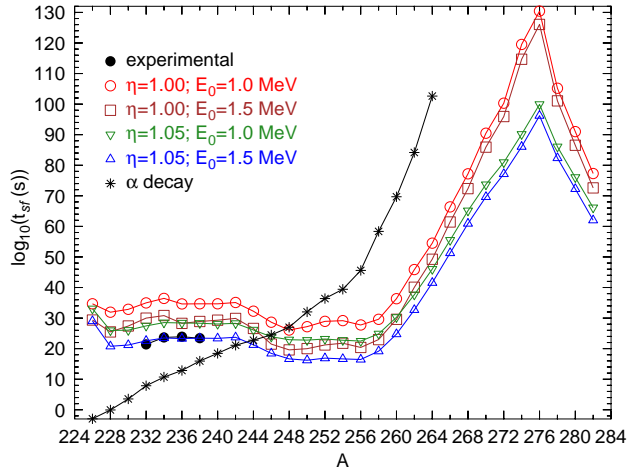


Figure 7. (Color online) Experimental  $t_{sf}$  half lives (bullets) are compared to different theoretical results (open symbols, fission; asterisk  $\alpha$ -decay) for the uranium isotopes up to the drip line nucleus  $^{282}\text{U}$ .

We observe the ground state evolution from a quadrupole deformed ground state in  $^{240}\text{U}$  with  $\beta_2 = 0.26$  to an spherical one for  $^{270}\text{U}$  (corresponding to  $N=178$ ) and for  $^{280}\text{U}$ . It is also worth mentioning the existence of a second fission isomer in  $^{240}\text{U}$  (excitation energy of 3.9 MeV) and  $^{250}\text{U}$  (excitation energy of 3.8 MeV, lower than the excitation energy of the first isomer). The situation in  $^{260}\text{U}$  is not as well defined as in the previous cases and there are three very shallow minima. The second one could be associated to the first fission isomer that is shifted to larger quadrupole moment values and zero octupole moment. Two fission isomers reappear in  $^{270}\text{U}$  but both are located at a very high excitation energy (around 9 MeV) and different quadrupole deformations than the ones in the light uranium isotopes. As a consequence of the increasing height and widening of the fission barriers as the neutron number approaches the neutron drip line we expect increasing  $t_{sf}$  values as can be observed in the next figure. In Fig 7 the spontaneous fission half lives  $t_{sf}$  of the uranium isotopes and computed with different choices of the  $\eta$  and  $E_0$  parameters are plotted as a function of mass number  $A$ . As in previous cases, the  $t_{sf}$  values have been obtained with the GCM collective mass and not taking into account the effects of triaxiality in the first barrier. The usual range of up to 12 orders in magnitude depending on the choice of parameters is observed. However, the trend with mass number  $A$  is the same in all the four sets of parameters considered. This again gives us confidence on the validity of the conclusions extracted from the trends with  $A$ . A decrease in the  $t_{sf}$  values is observed up to mass number  $A=256$  where it becomes a steady increase with mass number up to  $^{276}\text{U}$

where the  $t_{sf}$  values reach a maximum that corresponds to a neutron number of 184 that corresponds to one of the classical magic numbers. The two neutron separation energy drops by 3 MeV in going from  $A=276$  (4.99 MeV) to  $A=278$  ( $S_{2N} = 1.94$  MeV what is a clear indication of extra stability. The half lives for this and the other isotopes beyond  $^{260}\text{U}$  are very large and the corresponding nuclei can be considered as stable against the spontaneous fission decay channel. As the BCPM functional has been created to give a reasonable description of the masses, it is reasonable to use its predictions for the binding energies of uranium and thorium to compute the half lives of  $\alpha$ -decay using the phenomenological Viola-Seaborg formula [56, 57]. The results for the uranium isotopes are plotted as asterisks in the figure. We observe a steady increase of  $t_{\alpha}$  with mass number that reaches its maximum at  $A=264$  where  $\alpha$  decay is no longer favorable energetically. From  $A=244$  on fission is faster than  $\alpha$  decay.

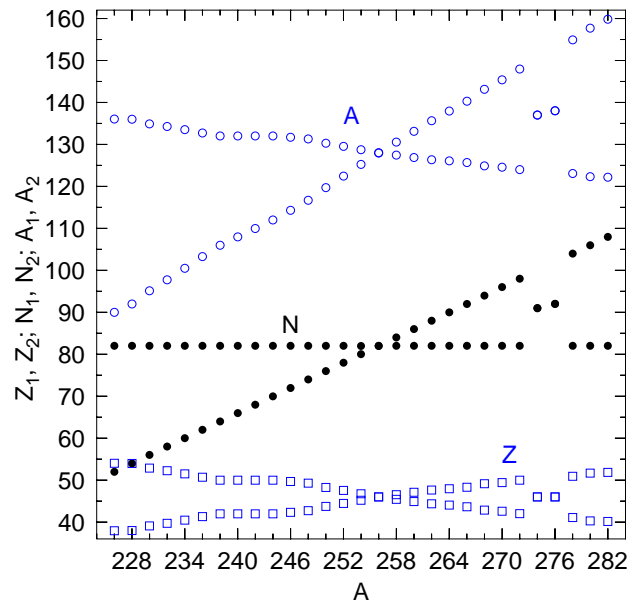


Figure 8. The number of protons ( $Z_{1,2}$ ), neutrons ( $N_{1,2}$ ) and mass number ( $A_{1,2}$ ) of the fission fragments is plotted as a function of the mass number  $A$  of the parent uranium isotope.

In Fig 8 the proton, neutron and mass numbers of the fragments in the fission of the uranium isotopes are plotted as a function of mass number  $A$ . Those numbers are obtained by integrating the densities of each of the fragments coming out of the two fragment (fusion valley) self-consistent solutions mentioned before and corresponding to the lowest energy. In some cases, there are additional fusion valleys with different fragments but they lie higher in energy. The issue of how to describe dynamically the evolution of the system through those valleys is a very interesting subject of research (see for instance [53]) with many practical applications (the real fission fragment mass distribution) but exceeds the scope of the present paper. The numbers discussed below are to

be taken as the ones of the peaks (most favorable mass) of the mass distribution of fragments prior to neutron emission. Except for  $^{274}\text{U}$  and  $^{276}\text{U}$  the number of neutrons in one of the fragments always corresponds to the magic number  $N=82$ . The neutron number of the other fragment varies linearly accordingly to the mass number of the parent. On the other hand, the number of protons, that is close to the magic number  $Z=50$  for the light isotopes (in good agreement with experiment [55]) varies linearly with mass number except for the isotopes  $^{238-244}\text{U}$  where it stabilizes at  $Z=50$  and for  $^{274}\text{U}$  and  $^{276}\text{U}$  (symmetric fission) where it is distributed equally between the two fragments. Also for the  $^{256}\text{U}$  isotope a symmetric splitting with equal fragments is obtained. Concerning the mass distribution of the fragments, the heavy fragment has a mass number around 136 for the light isotopes that decreases with the mass number of the parent until the  $^{256}\text{U}$  isotope is reached. At this point the mass number of the heavy isotope starts to increase linearly with the exception of  $^{274}\text{U}$  and  $^{276}\text{U}$ . This change in tendency is due to the increasing number of neutrons: as the number of neutrons increases, the fragment with  $N=82$  is no longer the heaviest one. In any case, the behavior beyond  $A=256$  is a rather academic issue as fission for those isotopes is a extremely unlikely process as discussed above.

#### IV. CONCLUSIONS

The fission properties of several actinides and super-heavy nuclei have been computed with the recently proposed BCPM EDF. The theoretical results for the spontaneous fission half lives show a large variability consequence of uncertainties in the evaluation of some parameters of the theory and also on the strong dependence of the collective inertia with pairing correlations. As a consequence of the large uncertainties in the theoretical results we are only able to compare with the experimental data trend with mass number (for instance the reduction by 27 orders of magnitude in the spontaneous fission half lives in going from  $A=232$  to  $A=286$ ). The theoretical

predictions seem to reproduce such trend giving us confidence in the convenience of the method and EDF for the study of fission properties of neutron rich uranium isotopes. There we find that the spontaneous fission half lives remain more or less constant up to  $A=260$  where they increase enormously as a consequence of the proximity to the magic neutron number  $N=184$ . Therefore, it is confirmed the prevalence of this magic number in an extreme neutron rich case. On the other hand, a comparison of the parameters defining the potential energy surface for fission (inner and outer barrier heights and fission isomer excitation energies) with the model dependent "experimental data" show a rather good agreement that gives us additional confidence on the validity of our conclusions. The results obtained clearly show that more attention has to be paid to a proper description (including beyond mean field effects) of pairing correlations in the configurations relevant to fission. The evaluation of the quasi-fission valley in the HFB model also allows to predict the peaks of the mass distribution of fission fragments. It is shown that the magic proton number  $Z=50$  and the magic neutron number  $N=82$  play an important role in determining the mass of the fragments.

To conclude, our study has shown the applicability of the BCPM EDF for fission studies in heavy and super-heavy nuclei. We have also pointed out the large variability of the theoretical predictions to the models used to evaluate the relevant parameters. However, this variability seems to respect the trend with mass number of the spontaneous fission half life and therefore we have applied our method to study fission properties of the uranium isotopes up to the neutron drip line. It is shown that beyond  $A=264$  the uranium isotopes can be considered as stable against fission and  $\alpha$ -decay.

#### ACKNOWLEDGMENTS

Work supported in part by MICINN grants Nos. FPA2012-34694, FIS2012-34479 and by the Consolider-Ingenuo 2010 program MULTIDARK CSD2009-00064.

- 
- [1] H.J. Krappe and K. Pomorski, *Theory of Nuclear Fission*, Lect. Notes in Phys. **838** (2012).
  - [2] D.N. Poenaru, *Nuclear decay modes*, Institute of Physics Publishing (1996).
  - [3] Hans J. Specht, Rev. Mod. Phys. **46**, 773 (1974); S. Björnholm and J. E. Lynn, Rev. Mod. Phys. **52**, 725 (1980); "Fifty Years of Fission", Nucl. Phys. **A502** (1989).
  - [4] M. Brack, J. Damgaard, A.S. Jensen, H.C. Pauli, V.M. Strutinsky and C.Y. Wong, Rev. Mod. Phys. **44**, 320 (1972).
  - [5] J. Decharge and D. Gogny, Phys. Rev. **C 21**, 1568 (1980).
  - [6] J.F. Berger, M. Girod and D. Gogny. Nucl. Phys. **A428**, 23c (1984).
  - [7] N. Nikolov, N. Schunck, W. Nazarewicz, M. Bender and J. Pei, Phys. Rev. **C83**, 034305 (2011).
  - [8] J. McDonnell, N. Schunck and W. Nazarewicz, arXiv: 1301.7587 (2013).
  - [9] P. Ring and P. Shuck, *The Nuclear Many Body Problem* (Springer-Verlag Edt. Berlin, 1980).
  - [10] M. Bender, P.-H. Heenen, and P.-G. Reinhard, Rev. Mod. Phys. **75**, 121 (2003).
  - [11] J. Erler, K. Langanke, H.P. Loens, G. Martinez-Pinedo, and P.-G. Reinhard Phys. Rev. **C85**, 025802 (2012).
  - [12] A. Staszczak, A. Baran and W. Nazarewicz, arXiv:1208.1215 (2012).

- [13] J.L. Egido and L.M. Robledo, Phys. Rev. Lett. **85**, 1198 (2000).
- [14] M. Warda, J.L. Egido, L.M. Robledo and K. Pomorski, Phys. Rev. **C 66**, 014310 (2002); Intl. J. of Mod. Phys. **E 13**, 169 (2004).
- [15] J.-P. Delaroche, M. Girod, H. Goutte and J. Libert, Nucl. Phys. **A 771**, 103 (2006).
- [16] N. Dubray, H. Goutte, and J.-P. Delaroche, Phys. Rev. **C77**, 014310 (2008).
- [17] V. Martin and L.M. Robledo, Int. J. Mod. Phys. **E 18**, 788 (2009).
- [18] S. Perez-Martin and L.M. Robledo, Int. J. Mod. Phys. **E 18**, 861 (2009).
- [19] W. Younes and D. Gogny, Phys. Rev. **C 80**, 054313 (2009).
- [20] H. Abusara, A.V. Afanasjev and P. Ring, Phys. Rev. **C82**, 044303 (2010).
- [21] B.N. Lu, E.G. Zhao and S.G. Zhou, Phys. Rev. **C85**, 011301 (2012).
- [22] A.V. Afanasjev, arXiv: 1303.1206 (2013).
- [23] M. Baldo, L.M. Robledo, P. Schuck and X. Viñas, Physical Review **C87**, 064305 (2013).
- [24] M. Baldo, P. Schuck, and X. Viñas, Phys. Lett. B **663**, 390 (2008).
- [25] M. Baldo, L.M. Robledo, P. Schuck, and X. Viñas J. of Phys. **G37**, 064015 (2010).
- [26] L.M. Robledo, M. Baldo, P. Schuck and X. Viñas, Phys. Rev. **C77**, 051301(R) (2008).
- [27] L.M. Robledo, M. Baldo, P. Schuck and X. Viñas, Phys. Rev. **C81**, 034315 (2010).
- [28] E. Garrido, P. Sarriguren, E. Moya de Guerra, and P. Schuck, Phys. Rev. C **60**, 064312 (1999).
- [29] M. Baldo, C. Maieron, P. Schuck, and X. Viñas, Nucl. Phys. **A736**, 241 (2004).
- [30] G. Taranto, M. Baldo and G.F. Burgio, arXiv: 1302.6882 (2013).
- [31] L.M. Robledo, *HFBaxial computer code* (2002).
- [32] L.M. Robledo and G.F. Bertsch, Phys. Rev **C84**, 014312 (2011).
- [33] M. Girod and B. Grammaticos, Nucl Phys. **A330**, 40 (1979).
- [34] M.J. Giannoni and P. Quentin, Phys. Rev. **C21**, 2060 (1980); M.J. Giannoni and P. Quentin, Phys. Rev. **C21**, 2076 (1980).
- [35] J. Libert, M. Girod, and J.-P. Delaroche, Phys. Rev. **C60**, 054301 (1999).
- [36] A. Baran, J.A. Sheikh, J. Dobaczewski, W. Nazarewicz, and A. Staszczak, Phys Rev **C84**, 054321 (2011).
- [37] G.F. Bertsch and H. Flocard, Phys. Rev. C **43**, 2200 (1991).
- [38] J.L. Egido and L.M. Robledo, Lecture Notes in Physics **641**, 269 (2004).
- [39] S. Goriely, S. Hilaire, M. Girod, and S. Perú, Phys. Rev. Lett. **102**, 242501 (2009).
- [40] R. Rodríguez-Guzmán, P. Sarriguren, L.M. Robledo, S. Perez-Martin Phys. Lett. **B 691**, 202 (2010).
- [41] L.M. Robledo, R. R. Rodríguez-Guzmán and P. Sarriguren Phys Rev **C 78**, 034314 (2008).
- [42] R. Rodríguez-Guzmán, P. Sarriguren, L.M. Robledo, and J.E. García-Ramos Phys. Rev. **C 81**, 024310 (2010).
- [43] L.M. Robledo and G.F. Bertsch, Phys. Rev. **C84**, 054302 (2011).
- [44] M. Warda and L.M. Robledo, Phys. Rev. **C 84**, 044608 (2011).
- [45] P. Möller, and A. Iwamoto, Phys. Rev. **C 61**, 047602 (2000).
- [46] P. Möller, D.G. Madlan, A.J. Sierk and A. Iwamoto, Nature **409**, 785 (2001).
- [47] L.M. Robledo, Intl. J. of Mod. Phys. **E16**, 337 (2007).
- [48] L.M. Robledo, J. of Phys. **G37**, 064020 (2010).
- [49] B. Singh, R. Zywina, and R. Firestone, Nucl. Data Sheets **97**, 241 (2002).
- [50] R. Capote *et al.* Nucl. Data Sheets **110**, 3107 (2009).
- [51] N.E. Holden and D.C. Hoffman, Pure Appl. Chem, **72**, 1525 (2000).
- [52] L. Dematté, C. Wagemans, R. Barthélémy a, R D'hondt, and A. Deruytter, Nucl. Phys. **A 617**, 331 (1997).
- [53] H. Goutte, J.F. Berger, P. Casoli and D. Gogny, Phys. Rev. **C 71**, 024316 (2005).
- [54] D. C. Hoffman, and M. M. Hoffman, Annu. Rev. Nucl. Sci. **24** 151 (1974).
- [55] K.-H. Schmidt *et al*, Nucl. Phys. **A 665**, 221 (2000).
- [56] V. E. Viola Jr. and G. T. Seaborg, J. Inorg. Nucl. Chem. **28**, 741 (1966).
- [57] T. Dong and Z. Ren, Eur. Phys. J. . **A 26**, 69 (2005).